

Failure Analysis of a Failed Anchor Chain Link

Sridhar Idapalapati^{1*}, Alfred R Akisanya², Kelvin M. Loh³ and Stedston Yeo³

¹ School of Mechanical and Aerospace Engineering, Nanyang Technological University, 50 Nanyang Avenue, Singapore 639798, Singapore.

² School of Engineering, University of Aberdeen, Aberdeen AB24 3UE, UK.

³ Professional Testing Services Pte Ltd, 32 Kian Teck Road, Singapore 628779, Singapore.

(Accepted for publication in Engineering Failure Analysis, 4 March 2018)

ABSTRACT

The failure of a metal chain link with stud during an anchoring operation of a ship is examined. Visual observation, optical and scanning electron microscopy analyses of the fracture surfaces in combination with hardness and tensile tests are used to establish the cause of failure. The chemical element composition, tensile strength, yield strength and elongation of the base metal of the chain link are within the recommended design values. However, cross-sectional microstructure examination revealed that the fracture occurred along the flash butt weld and initiated from a pre-existing edge radial crack on the outer surface which had been painted over. The presence of inclusions near the outer surface, decarburized boundaries of the inclusions and decarburized thin strip along the entire weldment had resulted in reduction in the strength of the weldment and subsequent initiation of the surface crack. The main cause of the chain link failure is improper flash welding and heat treatment resulting in localised carbide segregations and embrittlement, leading to initiation of surface crack and consequent overload of the remaining net-section area of the chain. There was no evidence of fatigue crack growth. Better inspection and maintenance would have led to early detection of the surface crack during any the periodic non-destructive testing.

Keywords: anchor chain link, failure analysis, weldment, microscopy.

*Corresponding author: msridhar@ntu.edu.sg

1. INTRODUCTION

Chain links are one of the important mechanical elements for securing a ship to a mooring or an anchor and in lifting operations. Metal chain links are manufactured from a straight solid rod that is bent into an oval shape; the ends are then flash welded together. To make the next chain in the link, a straight solid rod is passed through the previously made link before bending and flash welding the ends. The process is repeated until the required length of the chain is attained. Post-welding heat treatment is carried out to relieve the residual stresses and control the microstructure associated with the welding process. Chain links are made with or without studs (see Fig 1). For studded chains, the stud is welded across the width of the chain link to provide additional structural rigidity. In practice, the welding process parameters are chosen to ensure the flash butt and the stud welds do not become the weakest parts of the link [1].

The integrity of a chain link depends not only on the material and manufacturing process but also on the stress state developed in the chain due to the load cycle in service. The stress distribution in a chain link when subject to tension or a combination of tension and bending can be determined using small deformation beam theory or finite element analysis; bending reduces the load carrying capacity of chain links, see for example [2-4]. Elastic-plastic analysis carried out by Pacheco et al. [5] showed that the compressive residual stress associated with proof loading of chain links improves the fatigue resistance. These previous analyses do not take into consideration the interaction between the microstructure of the weld and the service environment which has been attributed to some recent chain link failures.

The failure of a Grade 80 metal chain link used for towing heavy-duty military vehicles initiated from the flash butt weld due to weld defects, improper post-weld heat treatment that resulted in a decrease in material hardness and corrosion resistance, coupled with fatigue loading [6]. Sujata et al. [7] concluded that the failure of a conveyor chain link was due to pre-existing surface defects in the billet used to make final chain link product. The analysis of fifteen separate failures of mooring lines at Norwegian Continental Shelf between 2010 and 2013 concluded that the failures

were caused by a combination of overload, fatigue and mechanical defects [8]. The failure incidents reviewed in [8] included a 76 mm diameter mooring chain on Transocean Winner semi that failed in 2010 at an applied tension of 2,100 kN while the ultimate failure load of the chain was about 6,100 kN; and the anchor chain link on Songa Dee semi that failed in 2011 at a load of 4,600 kN while the break load test on pieces of the chain link gave a failure load of 6,030 kN.

In the present study, we report the investigation of the failure of a 73 mm nominal diameter Grade U3 anchor steel chain link with studs and nominal breaking load of 3,988 kN. The failed chain was provided by a shipping operator, claiming the anchor chain was installed as new and used in anchoring operations of a double hull oil and chemical tanker. The failure occurred at the port in a 30 m of water during the anchoring operation of the tanker show total weight was 475 TN (48,535 MTons). The tanker approached the port as normal at about 1.5 knots, swinging to port against a water current of about 2 knots. Soon after the anchor was let go, it was noticed that the anchor brake was not holding. The anchor chain went tight as the tanker was drifting; the chain could not hold the vessel and this resulted in the failure of the chain links. Nine (9) shackles and the failed chain link were lost into the sea. The failed chain link was subsequently recovered from the seabed, and appeared to have failed at the flash weld and the also the stud weld. In-depth analysis, involving visual and microscopic examination using scanning electron microscope (SEM) combined with hardness and tensile tests, is carried out in this study to establish the root cause of failure and make recommendations on how to prevent such failure are made.

2. FAILURE ASSESSMENT

2.1 Visual examination

One set of the failed anchor chain link and the associated stud, hereafter referred to as the ‘sample’, is shown in Fig 2b,c. Prior to the failure, the stud link would have been attached to the anchor chain link, at the mid length of the chain, via a fillet weld with one end of the stud welded over and across the flash butt weldment of the anchor chain link, as per the schematic shown in Fig 1. The effect of the interaction between the chain link flash butt weld and the chain link-stud weld on the failure of the chain link is explored in the current study.

For descriptive purpose, the following abbreviated naming of the fracture surfaces is adopted:

- i. **Fracture Surface A** - Primary fracture surface located at one end of the anchor chain link, mating with fracture surface B (Fig. 2a,b & 3a).
- ii. **Fracture Surface B** - Primary fracture surface located at the other end of the anchor chain link, mating with fracture surface A (Fig. 2a,b & 3a).
- iv. **Fracture Surface C** - Fracture surface located on the end of the stud link that was welded to chain link on the opposite end of the flash weld, and mating with fracture surface D (Fig 2a,c)
- v. **Fracture Surface D** - Found on the inner perimeter and middle length of the anchor chain link, mating with fracture surface C. (Fig 3b)
- iv. **Fracture Surface E** - Fracture surface located on the other end of the stud link that was welded over and across the chain link flash weld, and mating with fracture surface F (Fig 2a,c)
- v. **Fracture Surface F** - Found on the inner perimeter and mid length of the anchor chain link at the location of the chain link failure, mating with fracture surface E (Fig 2a & 3c)

As noted above, the mating pairs of fracture surfaces are A and B (both on the chain link); C and D (with C on the stud and D on the inner perimeter of the chain link) and E and F (with E on the stud and F on the inner perimeter of the chain link), see Figure 2a

A detailed visual examination was performed on the sample before any further investigation was carried out. We note that the sample was covered with multiple layers of rust and black coloured paint-like coating on its surface. Most of the paint had been flaked off revealing the uniformly corroded base metal.

The occurrence of failure at the weld revealed the presence of pre-existing defect before the final failure and significant level of corrosion. Relatively fresh, shining mating fracture surfaces were found at the two fractured surfaces A and B at the ends of the anchor chain link (Fig 3a). In addition, two corroded mating fracture surfaces were found where the stud link was welded to the anchor chain link (Fig 3b,c).

2.2 Dimensional Measurements

The original shape of the anchor chain link appeared to be extensively plastically deformed. Thus, a series of dimensional measurements of the sample were taken and the results are shown in Table 1. The location of the measurements on the chain link is indicated in Fig. 2b and diameters 1 and 2 are the minimum and maximum measurement at a given location respectively. Note that the nominal diameter of the chain link was 73 mm.

From the measurements obtained, there are significant deviations between the two diameters at almost every point considered except for Point 4 which had the smallest deviation. According to the measurement record of the anchor chain provided by the operator, the worst measurement obtained for the body of the chain link four months prior to the failure was 69.7 mm. Except for Point 4, all Chain Diameter 1 values from the anchor chain link were smaller than the worst measurement recorded. The significant difference between Chain Diameter 1 values and Chain Diameter 2 values was likely the result of a combination of extensive plastic deformation and corrosion. Another possible reason for the significant difference in the diameters at Fracture Surface D would be the inherent smaller local diameter of the chain link at location 4 due to the pre-existing groove where the stud end was welded onto the chain link (Fig 3b); the diameter at this location would not have been recorded by the operator because of the obstruction from the stud link

2.3 Macroscopic examination of the fracture surfaces

Fracture Surfaces A and B – Primary Fracture Surface

Macroscopic examination was performed on the primary fracture surfaces of the sample using a low magnification stereo microscope to scrutinize the characteristics of the fracture. The two mating fracture surfaces A and B exhibited similar features in terms of characteristics, size, topography and colour intensity, see Fig. 3a, c. Both fracture surfaces had a mostly flat topography, except for a small crater in the middle of Fracture Surface A (Fig 4). The mating surface in the middle of fracture surface B was slightly popped out (Fig 3c). In addition, there were jagged shear lips found on the inner circumference of the fracture surface of the chain link directly beneath the contact surface with the stud (Fig. 3a, c).

Three distinct regions with different colour intensities were found on Fracture Surfaces A and B namely:

- (i) Black Region – approximately a quarter of the outermost facing part of the surface was covered by a black-coloured paint-like coating up to a radial depth of 15 mm (Fig. 3a and Fig. 4). Small amount of brownish-orange deposits, appearing to be rust, were present on the coating. This is indicative of a relatively deep edge crack that existed on the surface of the chain link prior to the final failure and had been painted over without the presence of the edge crack being noticed during any of the condition monitoring inspections. With a quarter of the fracture surface covered in this black-coloured paint, there would have been a significant reduction in the available net section surface area of the material to support the applied loads. This pre-existing defect is a possible origin of final fracture of the chain link. Microscopic examination described below was used to further assess the origin of this surface crack, e.g. if it was due to fatigue loading or not.

- (ii) Silver Region - the primary fracture surface was predominantly shining and silver-coloured at the centre of the surface; this is indicative of a fresh fracture (Fig 3a & Fig 4).
- (iii) Light Brown Region - there was a light brown colour region on fracture surface A but not on fracture surface B. A set of photographs of the failed chain were taken onsite about one hour after the fracture occurred. The failed chain was received for analysis two months after the incident, and another set of photographs were taken. A comparison of the two sets of photographs revealed that the light brown region present on fracture surface A was probably due to post-fracture corrosion that took place in the intervening time between the incident and the samples being made available for analysis.

Fracture Surfaces C and D

Scrutiny of the remnants of fillet weldment of the stud to the chain link revealed that the two mating fracture surfaces C and D formed one of the joints that connected the stud link to the anchor chain link at the other side of the chain flash weld. Fracture Surface D exhibited an oval shape located at the mid length and inner perimeter of the anchor chain (Fig 3b). The oval shape of fracture surface D on the inner surface of the chain link was surprisingly found to be bigger than the corresponding mating fracture surface C on the stud. This is indicative of failure of the stud link – chain link weld failure preceding plastic deformation at the inner perimeter of the anchor chain link. Both fracture surfaces and the area bounded by the fracture surfaces were severely corroded. Examination of the as-received photograph taken an hour after fracture revealed a silver fracture surface suggestive of a fresh fracture.

2.4 Microscopic examination of the fracture surfaces

Microscopic examination of the fracture surfaces was conducted in accordance to ASTM E3-2001 [9] using a high magnification optical microscope. The analysis was performed on prepared longitudinally cross-sectioned specimens extracted from the primary fracture surfaces (Fig. 5). The etchant used was 3% Nital solution. The cross sectional view of the fracture surfaces was examined to determine the fracture profile (crack origin, propagation and final rupture) and the thermomechanical processing.

Microstructural examination of the base metal revealed a tempered martensitic microstructure (lighter etched phase) with longitudinal heavily banded lines (darker etched phase) of carbides (Fig 5). The bandings were particularly segregated near the centre of the chain link. Sulphide-type stringers were also observed in the longitudinal direction. The cross-section of the fracture surface was relatively flat, except for the crater in the middle and a shear lip on the inner edge of chain directly beneath the stud weld (Fig 5b). A thin strip of decarburized weldment (whiter etched phase) was found on the fracture surface, particularly at the inner and outer perimeter of the chain link (Fig 5c).

Scrutiny of the suspected fracture origin at the outer circumference (corresponding to the black region on Fracture Surface A) revealed a black colour paint-like coating without decarburization. Beneath the paint-like coating, multiple greyish crack-like inclusions with decarburized boundaries (whiter etched phase) appeared to have penetrated perpendicularly from the fracture surface (Fig. 5d). These crack-like inclusions are connected to the thin strip of decarburized weldment (Fig. 5e).

At the heat-affected zone (HAZ) near the inner and outer circumference, carbide segregation appear to be located at austenite grain boundaries (Fig 5c). At the crater (corresponding to the mid thickness crater on Fracture Surface A), fine secondary cracks appeared to propagate along the heavily segregated longitudinal banding lines (Fig 5d).

Microstructural examination of fracture surface B revealed similar observations at the base metal and the fracture surface as those seen on fracture surface A, particularly the presence of inclusions and decarburization. In addition, remnants of welding fins were observed at the outer diameter.

There was no evidence of any fatigue damage on the chain link and stud link fracture surfaces.

2.5 Scanning Electron Microscopy (SEM) Examination and Energy-dispersive X-ray Spectroscopy (EDX) Analysis

Scanning Electron Microscopy (SEM) Examination

SEM analysis was performed on fracture surface A to further confirm the fracture profile, i.e. crack origin, propagation and final rupture. The locations on the fracture surface where SEM analysis was performed are shown in Fig 6.

In particular, the three distinct regions of different colours observed during the macroscopic examination were also observed under SEM. At the black region (location 1 in Fig 6a), the paint-like coating covered nearly a quarter of the fracture surface, hindering the identification of any fracture features without having to remove the paint. We believe this section of the fracture surface is a pre-existing edge crack not noticed during any of the inspections and has been painted over. There were surface cracks on the paints (Fig 6b) which would have led to ingress of water and corrosion. This was further confirmed by the cleavage facets found at location 2 (see Fig 6a) amidst the corrosion deposits where the painting has been exposed (Fig. 6c).

At the light brown region (location 3 in Fig 6a), a brittle fracture morphology similar to the silver region (location 4 in Fig 6a) was observed. However, corrosion deposits rendered most of the fracture features unidentifiable. Small shear dimples were observed on the shear lips at the circumference (Fig. 6d) while at the silver region (location 4 in Fig 6a), brittle cleavage facets were observed (Fig. 6e).

Electron Dispersed X-ray Spectrometry (EDX) Analysis

Semi-quantitative EDX analysis was conducted, in accordance with ASTM E1508-98 (Reapproved 2003) [10] using an EDX analyzer coupled to the SEM machine on a cross-sectioned fracture surface A for elemental identification at key locations on the surface. The EDX results for the paint-like coating on the fracture surface, at the inclusion and at the light grey inclusion/base metal boundary are shown in Fig 7,

For the paint-like coating present at the black region of fracture surface A, a major presence (>10 mass%) of iron, oxygen and a minor presence (< 10 mass%) of carbon and manganese were detected (Fig 7a). We note that the element composition of the paint present on the outer circumference of the chain link (not shown) was similar to that found on the fracture surface; this further confirms that the pre-existing crack was not detected when the painting was carried out.

For the light grey nodules (i.e. the inclusions), a major presence (> 10 mass%) of iron, oxygen, manganese and a minor presence (< 10 mass%) of carbon and titanium was detected (Fig. 7b); while for the light grey boundary separating the inclusion and base metal, a major presence (>10 mass%) of iron, oxygen and a minor presence (< 10 mass%) of carbon and manganese were detected. The high amount of iron and oxygen content in the inclusions and paint-like coating suggest that they likely consisted of a high amount of corrosion deposits within it.

2.6 Element composition analysis

Chemical analysis was conducted in accordance to ASTM E415-2008 [11] using an optical emission spectrometer. The test was performed on cross-sectioned specimens extracted from the base metal of the anchor chain link and stud link. The results are presented in the Table 2.

According to the operator, the chain link material was from the same batch as the batch cast A and A; the element composition independently determined for these two batches by Lloyd's Register and the recommended design values for mooring and anchor chain [12] is included in Table 2. The results of the current analysis indicated that the composition of the carbon steel anchor chain

link was within the recommended specification by Lloyd's Register [12]. The marginally higher Nitrogen content for the cast numbers tested in the mill certificate was deemed not to have any significant effect. For the stud link, the carbon content met the requirements of maximum 0.33%.

2.6 Tensile Test

Tensile test was conducted, in accordance with ASTM A370-2011 [13] with a universal tensile machine (Model: Avery Denison 7157) to ascertain if there has been a deterioration of the uniaxial mechanical properties due to operational use. The test specimen was extracted from the core of the anchor chain link at the away from flash butt-welded section. The core of the anchor chain link was extracted as it was most likely to be the least plastically deformed portion that would give a more accurate result for the test. The tensile test results are summarised in Table 3.

The results of the tensile test and the mill certificate values were within the recommended design specifications by Lloyd's Register [12]. Consequently, lower than expected strength or excessive elongation of the cast chain link material is ruled out as contributing factors to the failure of the chain. However, due to the extensive plastic deformation of the chain link, work hardening of the plastically deformed region of the chain might have occurred and resulting in higher than expected strength locally.

2.7 Hardness Test

Vickers hardness test was conducted in accordance to ASTM E92-1982 (Reapproved 2003) [14] with a Vickers hardness tester (Model: Mitutoyo HV-114) using a 98.1 N load. The test was performed on longitudinally cross-sectioned specimens extracted from the primary fracture surfaces. The hardness was measured at 18 separate points on the cross section of fracture surface A and 14 points on the cross section of fracture surface B. In general, all the hardness measurement locations, shown in Figure 8, were 0.5 mm away from the edge or surface and 1.0 mm away from each other. The hardness values are provided in Table 4.

Based on ASTM A370-11 [13] approximate hardness conversion table for non-austenitic steels, a minimum tensile strength of 690 MPa recommended by Lloyd's Register for mooring and anchor materials [12] would correspond to an approximate minimum Vickers Hardness Number of 210. The HAZ, with the grain boundary carbide segregation, in the tested chain link generally exhibited a much higher hardness than the base metal. However, the flash butt weldment exhibited the lowest hardness rendering the weld to be the weakest part of the chain link.

3. DISCUSSION

The as-received sample consisted of an extensively plastically deformed fractured chain link with a fractured stud link at the fillet weld. The current investigation focused on the flash butt weldment of the chain link where the fracture was believed to have initiated. As the failure took place in India at mid-day (approximately 35 °C), the temperature of the environment is not believed to have any significant effect on the material properties or on the failure initiation.

The dimensions of the chain link measured for corrosion degradation monitoring purposes four months prior to the failure were found to be within the allowable diameter tolerance. However, the measurement of the as-received failed chain link indicated smaller diameter than during the corrosion degradation monitoring due to the extensive plastic deformation near the failure location. Further, the region where the stud link was welded to the chain link was found to have an average diameter that is slightly smaller (5% smaller) than the nominally specified value. This could lead to overestimation of the load carrying capacity of the chain link.

The chain link was most likely produced by rolling method as seen from the longitudinal bandings lines of carbides in the tempered martensitic microstructure. The element composition of the carbon steel chain link and stud as analyzed and as stated in the mill certificate were in accordance with the material requirements for anchor chains [12]. The tensile strength, yield strength and elongation of the chain link base metal were experimentally determined and also found to be within the recommended Lloyd's Register material requirements for anchor chains [12]. The element composition and uniaxial tensile properties of the base material of the chain link are therefore

indicative of appropriate level of strength and ductility in the base metal for the anchoring requirement.

There are two possible sources of stress experienced in the chain link at the flash butt weldment. The first possible source would be from the welding residual stress. The second possible source would be from service load in the form of longitudinal tensile loading and bending load during anchoring.

Based on the two distinct black (covered by paint-like coating) and silver (fresh fracture) regions on the fracture surface, the fracture appeared to have progressed in two separate occurrences at the flash weld from the outer surface radially towards the inner surface. Comparison of the two mating fracture surfaces A and B revealed that the fracture surface near the outer surface was corroded and covered by adherent paint-like coating; the exact mode of crack propagation of the first occurrence of cracking at the flash weld could not be ascertained. However, this paint-like coating at the crack origin and the circumference were devoid of decarburization which suggested that the paint-like coating was applied in the presence of a pre-existing crack. There was no evidence of striations on the crack surface suggesting it was not associated with fatigue loading. The pre-existing edge radial crack was significantly deep that the net-section area of the chain link was reduced by almost a quarter. This would have resulted in significant reduction in the load carrying capacity of the chain link and consequently in the final failure of the chain link. It is surprising that that the surface crack in the chain was not detected during any of the inspection or maintenance processes.

Cross-sectional microstructure examination revealed that the fracture occurred along the flash butt weldment. In particular, at the fracture surface, the presence of (i) inclusions near the outer surface; (ii) decarburized boundaries of the inclusions and (iii) decarburized thin strip along the entire weldment, would have synergistically conferred lower strength to the weldment region. In general, the flash butt weldment exhibited lower hardness than the base metal, rendering the weld to be the weakest part of the chain link. In addition, remnants of the flash butt welding fins found near the fracture origin might have acted as stress concentrations sites for crack initiation. Furthermore, the localized higher hardness at HAZ due to carbide segregation, appearing to be located at prior

austenite grain boundaries suggest possible improper welding or heat treatment temperature control. These carbide segregations might have acted as embrittling region promoting crack initiation.

As the chain link was not known to be exposed to any high temperature oxidizing environment during service, the observed decarburization along the weldment would have likely occurred during the flash butt welding process or during the welding of the stud to the chain link. With the inclusions extending from the thin strip of decarburized weld, it further suggested that the inclusions were trapped at the chain link butt surfaces and their boundaries decarburized during the welding process. In addition, the crack-like morphology of entrapped inclusions suggested the possible occurrence of minute cracks during the flash-butt welding process.

For the second occurrence of cracking, the tensile loading experienced by the anchor chain link likely resulted in the propagation of the pre-existing crack in a brittle manner across the weldment. Final ductile rupture via micro-void coalescence occurred at the shear lips near the centre of the of the cross section of the chain link when the remaining material was not able to sustain the loading, causing extensive bending away of the two separated chain link fracture surfaces. Subsequently, the stud link fractured at the fillet welding and broke off from the plastically deformed chain link body.

Flash butt welding, and post-welding heat treatment are inevitable aspects of the manufacturing process of a chain links. For chain links with a stud, the standard practice is to position the flash weld and the stud at mid-length of a chain link to ensure symmetrical deformation in operation. The potential stress concentration and variation in the material properties near the weld due to the welding process must be minimised. ASTM standard A391 [15] requires that a chain link at the time of shipment be free of discontinuities that could prevent the chain from sustaining the working load limit, while BS1834 [16] requires that the fins caused by flash welding be removed. Improper flash welding and heat treatment resulting in localised carbide segregations and embrittlement, coupled with the presence of weld fin and surface edge crack, in the chain link under consideration are major contributing factors that led to the failure of the chain when subject to normal working

load. This observation applies to other steel chain links with studs, see, for example, Grade 80 towing chain link [6].

4. CONCLUSION

Based on the review of available background information and results of tests performed, it was established that the underlying cause of chain link fracture was due to brittle overload, arising from a pre-existing crack. The pre-existing crack was most probably due to the lowered strength caused by welding inclusions and decarburization. Remnants of the flash butt welding fins found near the fracture origin and HAZ grain boundary carbide segregation might have also acted as stress concentrations sites for crack initiation. A more rigorous inspection and maintenance procedure of the chain link would have led to early detection of the surface crack before the total failure.

ACKNOWLEDGMENTS

ARA acknowledges the financial support of Binks Trust through funding made available to the School of Engineering, University of Aberdeen, UK.

REFERENCES

- [1] Kim DC, So WJ, Kang MJ. Effect of flash butt welding parameters on weld quality of mooring chain. *Archives of Materials Science and Engineering* 2009; 38: 112-117.
- [2] Otterson JE. Notes on chain cables. *Trans SAME* 1913; 21: 155-184.
- [3] Lerein J. Stress analysis of anchor chains. In: *Proc 6th International Offshore Mechanics and Artic Engineering Conference, Houston, Texas, 1987*; 1:221-226.
- [4] Papazoglou VJ, Katsaounis GM, Papaionnou JD. Elastic static analysis of chain links in tension and bending. In: *Proc 1st International Offshore and Polar Engineering Conference, Edinburgh, UK, 1991*; 3: 252-258.

- [5] Pacheco PMC, Kenedi PP, Jorge JCF. Elastoplastic analysis of the residual stress in chain links. In: Proc 21st International Offshore Mechanics and Arctic Engineering Conference, Oslo, Norway, 2002; 2: p39-46.
- [6] Al-Fadhlah K., Elhholy A., Majeed M. Failure analysis of Grade-80 alloy steel towing chain links. *Engineering Failure Analysis* 2010; 17: 1542-1550.
- [7] Sujata M., Venkatasawamy MA, Parameswara MA, Bhaumik SK. Failure analysis of conveyor chain links. *Engineering Failure Analysis* 2006; 13: 914-924.
- [8] Kvitrud A. Lessons learned from the Norwegian mooring line failures 2010-2013. In: Proc. 33rd ASME International Conference on Ocean, Offshore and Arctic Engineering, 2014, San Francisco, California, USA. OMAE2014-23095.
- [9] ASTM E3-2001. Standard practice for the preparation of metallographic specimens. ASTM, 2001.
- [10] ASTM E1508-98 (Reapproved 2003). Standard guide for quantitative analysis by energy-dispersive spectroscopy. ASTM, 2003.
- [11] ASTM E415-2008. Standard test method for atomic emission vacuum spectrometric analysis of carbon and low-alloy steel. ASTM 2008.
- [12] Lloyd's Register, *Rules for the manufacture, testing and certification of materials*. Lloyd's Register 2011. Chapter 10.
- [13] ASTM A370-2011. Standard test methods and definitions for mechanical testing of steel products. ASTM 2011.
- [14] ASTM E92-1982. Standard test methods for Vickers hardness and Knoop hardness of metallic materials. ASTM 1982.
- [15] ASTM A391-2001. Standard specification for Grade 80 alloy steel chain. ASTM 2001.
- [16] BS 1834. Short link chain for lifting purposes – general conditions of acceptance. British Standards Institution 1990.

LIST OF TABLES

- Table 1: Dimensional Measurements of the fractured chain link and stud.
- Table 2: Element composition of the base material of the chain link and stud link
- Table 3: Uniaxial tensile properties of the chain link material
- Table 4: Hardness of the weld and base material of the chain link and stud

LIST OF FIGURES

- Figure 1: Schematic of a chain link (a) without a stud and (b) with a stud
- Figure 2: (a) Schematic diagram of the failed anchor chain link showing the location of the fracture surfaces A, B, C, D, E and F, (b) the as-received failed anchor chain link and (c) the detached stud link. The locations of where the diameter is measured are indicated as Points 1, 2, 3 and 4.
- Figure 3: The failure surfaces. (a) Mating fracture surfaces A and B on the chain link, (b) fracture surface D and (c) fracture surface F.
- Figure 4: The different colour intensities on fracture surface A and the centrally located crater
- Figure 5: (a) Longitudinal cutting planes on fracture surface A; (b) longitudinal cross-section of fracture surface A along cutting plane 2; (c) magnified view of the shear lip, (d) magnified of the fracture initiation site showing the inclusion, and (e) longitudinal cross-section of the fracture surface along cutting plane 2.
- Figure 6: (a) Locations SEM analysis of fracture surface A and the corresponding SEM micrographs at (b) location 1, (c) location 2, (d) location 3, and (e) location 4.
- Figure 7: EDX analysis of different locations on fracture surface A
- Figure 8: Hardness test locations on the longitudinal cross-section of (a) fracture surface A and (b) fracture surface B.

Table 1: Dimensional Measurements of the fractured chain link and stud.

Location		Measurement (mm)	Standard specification (mm)	
Anchor Chain Link				
Fracture Surface A	Chain Diameter 1	69.22	73.00	
	Chain Diameter 2	73.08		
Fracture Surface B	Chain Diameter 1	69.43		
	Chain Diameter 2	73.11		
Body of anchor chain link	Point 1	Chain Diameter 1		70.99
		Chain Diameter 2		73.72
	Point 2	Chain Diameter 1		68.63
		Chain Diameter 2		70.88
	Point 3	Chain Diameter 1		68.57
		Chain Diameter 2		70.75
	Point 4	Chain Diameter 1	70.96	
		Chain Diameter 2	70.36	
Fracture Surface D	Chain Diameter 1	66.78		
	Chain Diameter 2	73.40		
Stud Link				
Fracture Surface C	Stud Diameter 1	61.48	Not Specified	
	Stud Diameter 2	71.44		
Stud link surface	Stud Diameter 1	67.79		
	Stud Diameter 2	58.45		
Middle of the stud link	Stud Diameter 1	48.90		
	Stud Diameter 2	56.27		
Length	Maximum Length	138.80		
	Minimum Length	118.23		

Table 2: Element composition of the base material of the chain link and stud link

Elements Analysed		Mass %				
		Anchor Chain Link Test Result	Stud Link Test Result	Lloyd's Register Certificate for Anchor Chain Cable and Chain Cable Fittings		Lloyd's Register [12]
				Cast A	Cast B	
Carbon	C	0.32	0.19	0.30	0.30	≤ 0.33
Phosphorus	P	0.025	0.016	0.016	0.022	≤ 0.04
Sulphur	S	0.004	0.009	0.005	0.013	≤ 0.04
Manganese	Mn	1.69	0.33	1.72	1.72	≤ 1.90
Silicon	Si	0.26	0.22	0.29	0.26	0.15 – 0.35
Chromium	Cr	0.10	0.15	0.12	0.15	≤ 0.25
Molybdenum	Mo	0.010	0.017	0.01	0.01	≤ 0.08
Nickel	Ni	0.049	0.066	0.12	0.11	≤ 0.40
Niobium	Nb	0.003	0.001	0.01	0.01	≤ 0.05
Aluminium	Al	0.038	0.011	0.030	0.027	≤ 0.065
Copper	Cu	0.18	0.14	0.14	0.11	≤ 0.35
Vanadium	V	0.006	0.002	0.01	0.01	≤ 0.10
Nitrogen	N	0.006	0.005	0.017	0.016	≤ 0.015

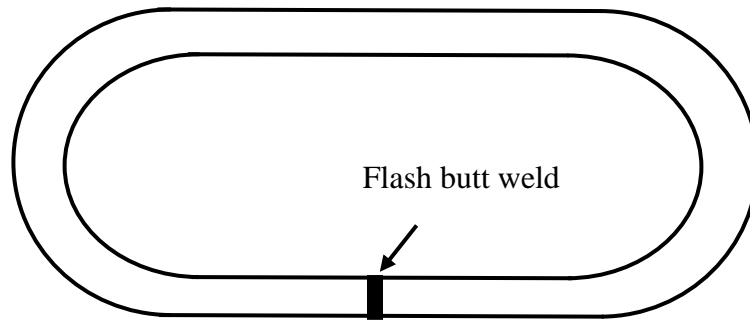
Table 3: Uniaxial tensile properties of the chain link material

Mechanical Properties	Test Result	Lloyd's Register Certificate for Anchor Chain Cable and Chain Cable Fittings for Cast A *	Lloyd's Register [9]
Ultimate Tensile Strength (N/mm ²)	699	708	≥ 690
0.2% Yield Strength (N/mm ²)	590	546	≥ 410
Elongation (%)	24	23	≥ 17

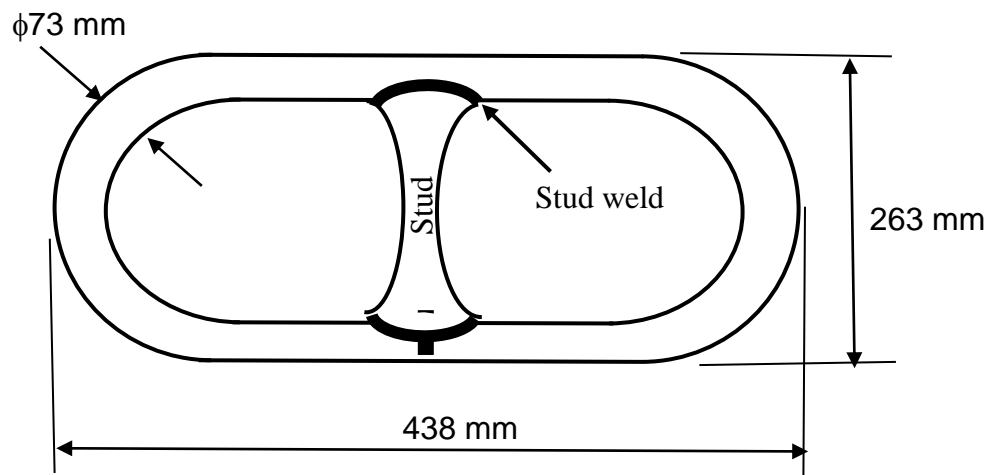
*The cast with the lowest tensile value was selected from the mill certificate for comparison.

Table 4: Hardness of the weld and base material of the chain link and stud

Vickers Hardness Number (HV) (Test Load Applied:10kgf)						
No	Fracture Surface A	Test Location	No	Fracture Surface B	Test Location	
1	303	HAZ	1	271	HAZ	
2	278		2	198	Weldment	
3	274		3	327	HAZ	
4	231	4	306			
5	234	Base Metal	5	287	Base Metal	
6	231		6	230		
7	217		7	229		
8	221		8	226		
9	219		9	224		
10	217		10	212		
11	224		11	214		
12	223		12	214		
13	220		13	204		
14	230		14	201		
15	224					
16	217					
17	194					
18	209					

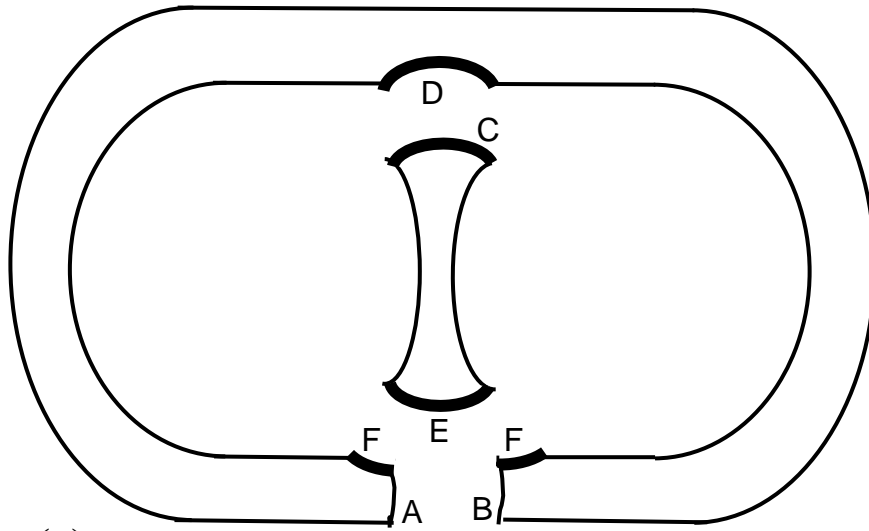


(a)

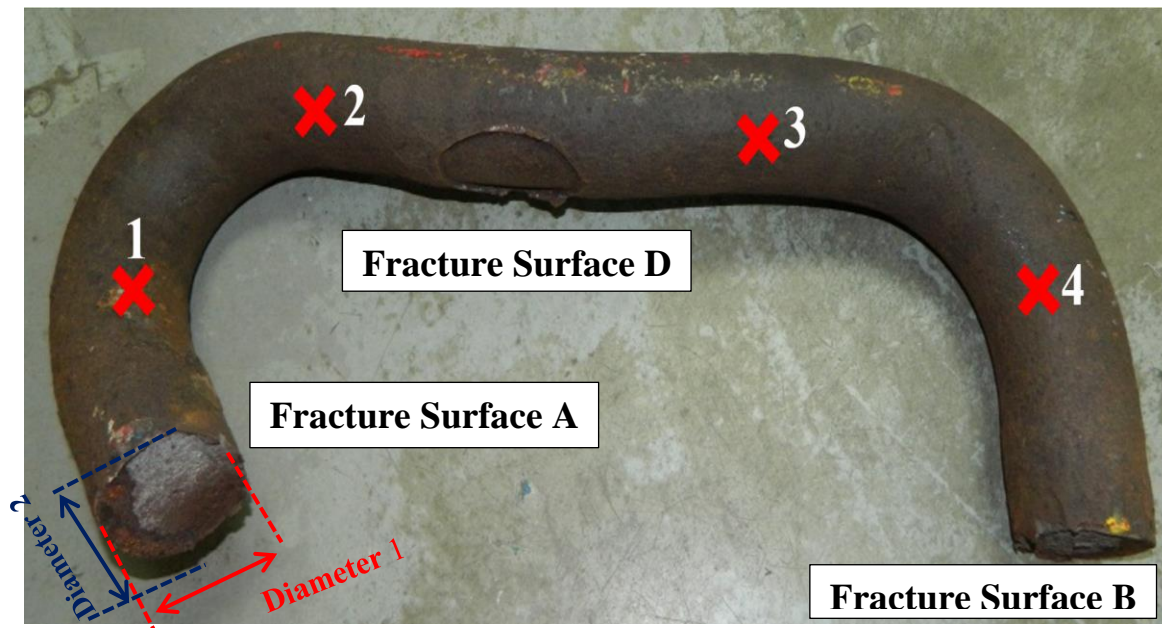


(b)

Figure 1: Schematic of a chain link (a) without a stud and (b) with a stud



(a)



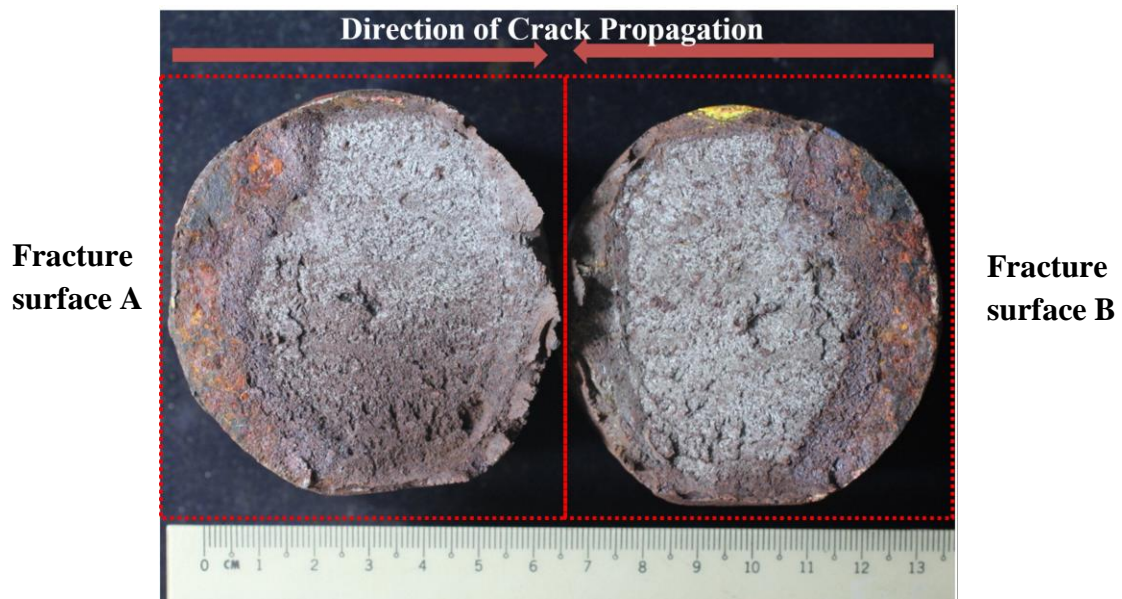
(b)

See next page for the caption for Figure 2.



(c)

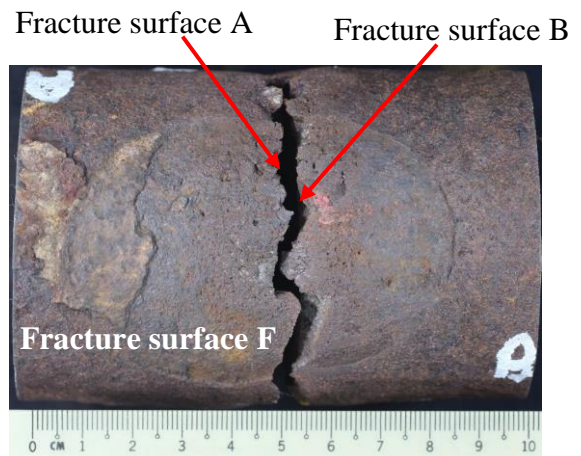
Figure 2: (a) Schematic diagram of the failed anchor chain link showing the location of the fracture surfaces A, B, C, D, E and F, (b) the as-received failed anchor chain link and (c) the detached stud link. The locations of where the diameter is measured are indicated as Points 1, 2, 3 and 4.



(a)



(b) Fracture surface D



(c) Fracture surface F

Figure 3: The failure surfaces. (a) Mating fracture surfaces A and B on the chain link, (b) fracture surface D and (c) fracture surface F.

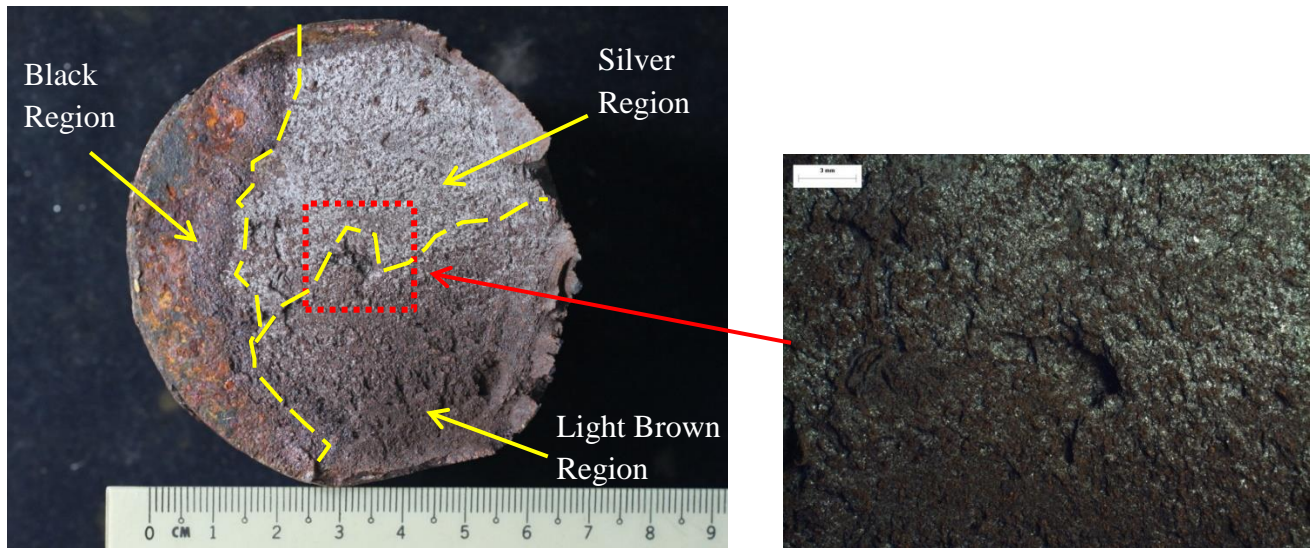
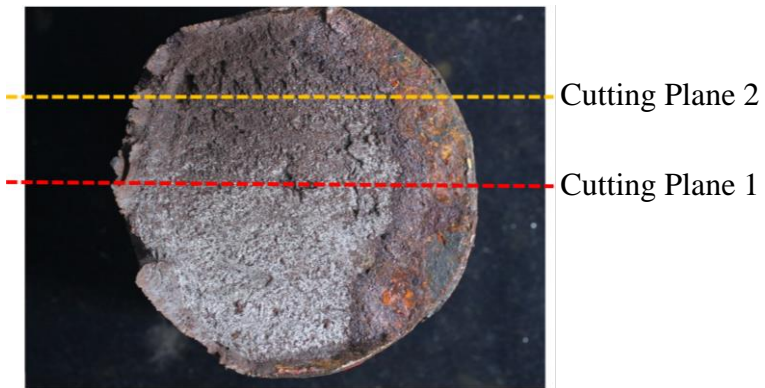
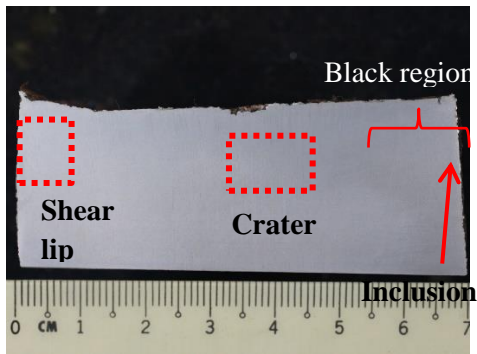


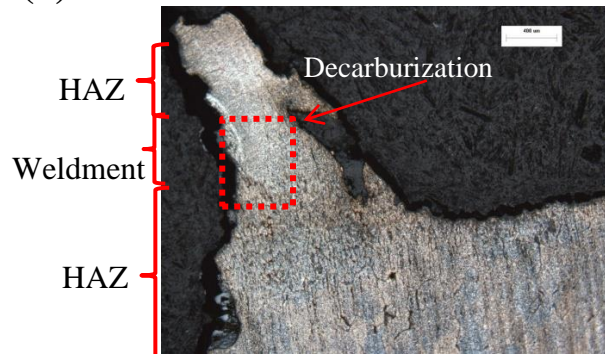
Figure 4: The different colour intensities on fracture surface A and the centrally located crater



(a)



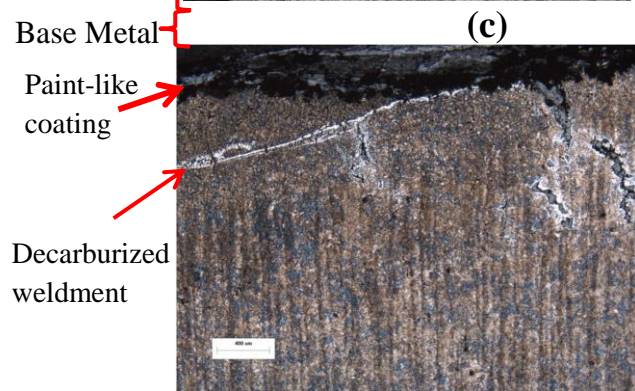
(b)



(c)

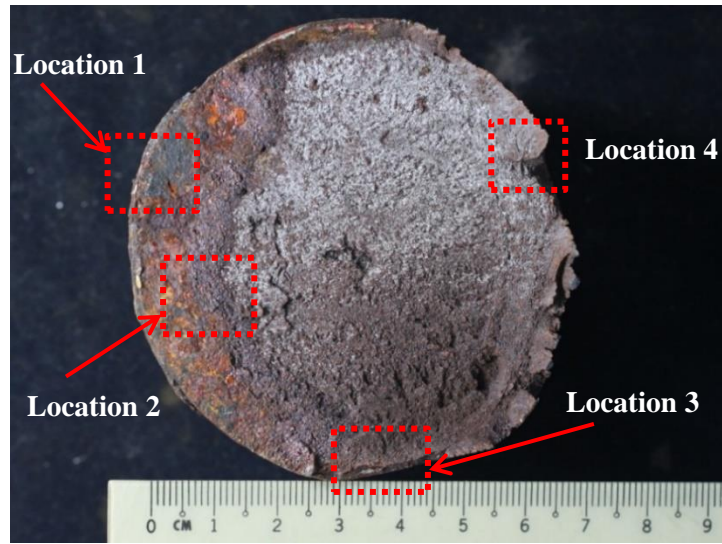


(d)

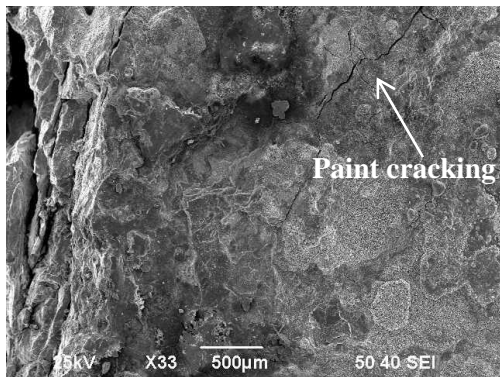


(e)

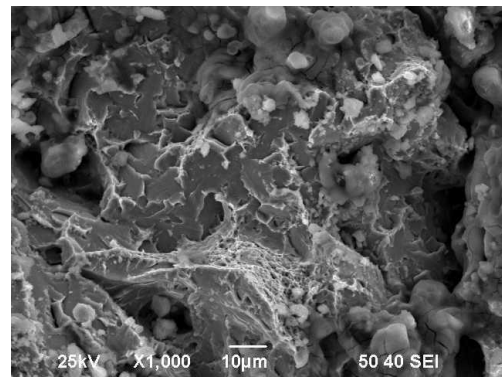
Figure 5: (a) Longitudinal cutting planes on fracture surface A; (b) longitudinal cross-section of fracture surface A along cutting plane 2; (c) magnified view of the shear lip, (d) magnified of the fracture initiation site showing the inclusion, and (e) longitudinal cross-section of the fracture surface along cutting plane 2.



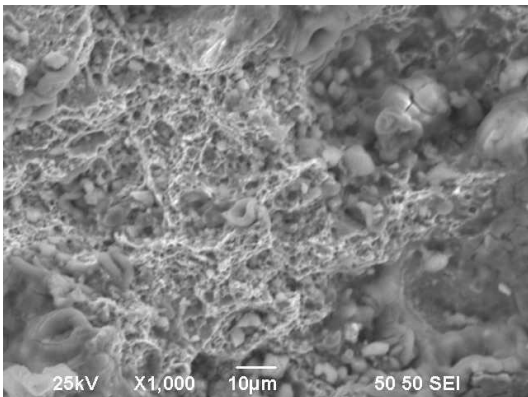
(a)



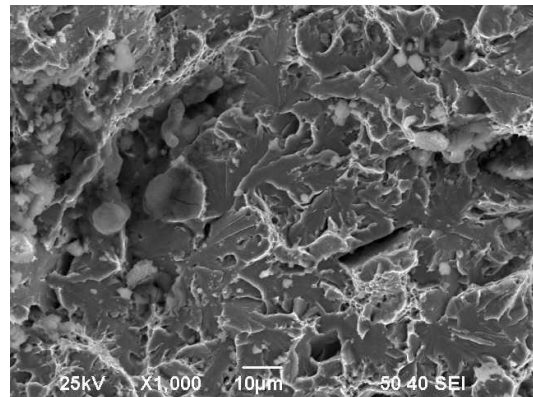
(b)



(c)

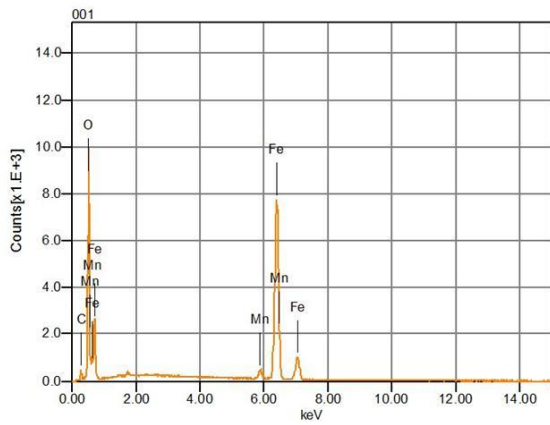
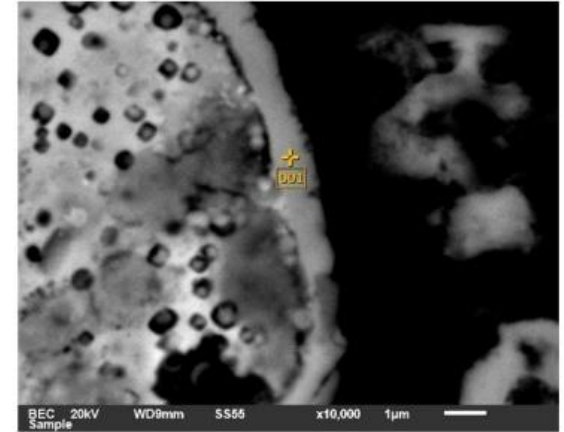
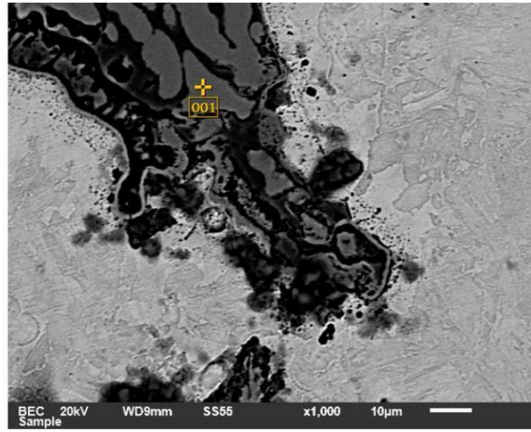
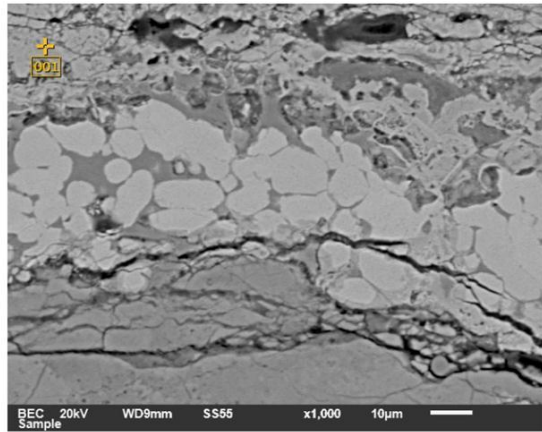


(d)



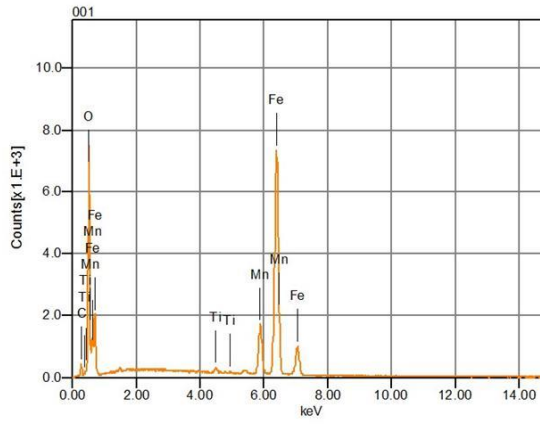
(e)

Figure 6: (a) Locations SEM analysis of fracture surface A and the corresponding SEM micrographs at (b) location 1, (c) location 2, (d) location 3, and (e) location 4.



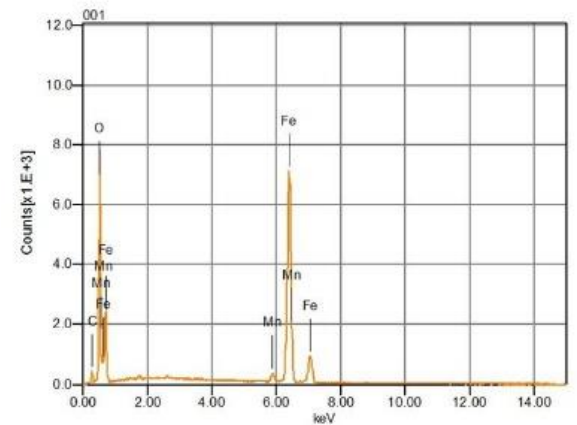
Chemical formula	mass%	Atom%	Sigma	Net	K ratio	Line
C	5.72	13.84	0.02	9809	0.0048256	K
O	28.54	51.89	0.04	239233	0.3996936	K
Mn	2.66	1.41	0.03	26300	0.0486541	K
Fe	63.08	32.86	0.09	551167	1.1793377	K
Total	100.00	100.00				

(a)



Chemical formula	mass%	Atom%	Sigma	Net	K ratio	Line
C	5.18	13.74	0.02	8561	0.0042116	K
O	22.46	44.78	0.04	178211	0.2977426	K
Ti	0.54	0.36	0.02	8288	0.0102449	K
Mn	11.37	6.60	0.05	109481	0.2025342	K
Fe	60.45	34.52	0.09	515220	1.1024212	K
Total	100.00	100.00				

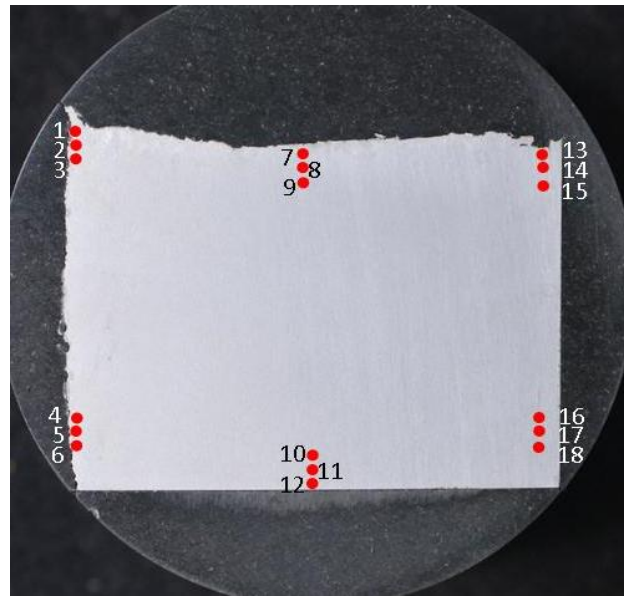
(b)



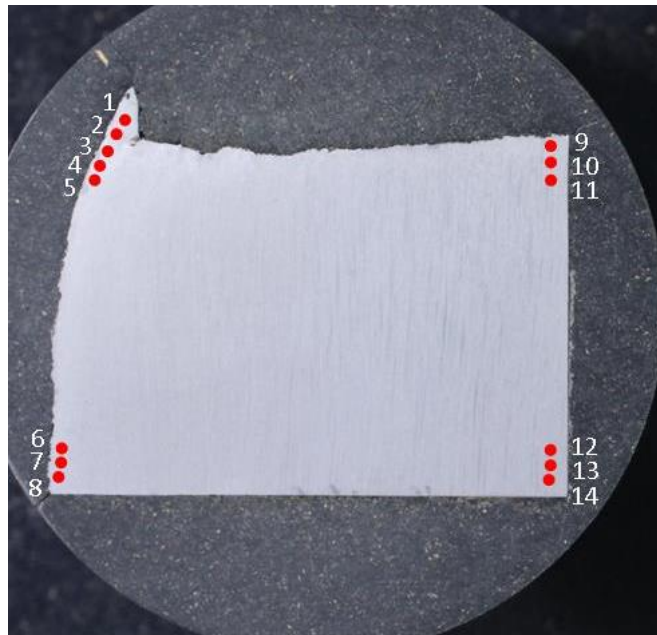
Chemical formula	mass%	Atom%	Sigma	Net	K ratio	Line
C	6.45	15.90	0.02	9722	0.0047828	K
O	26.10	48.31	0.04	188419	0.3147984	K
Mn	1.97	1.06	0.03	17223	0.0318621	K
Fe	65.48	34.73	0.10	506850	1.0845103	K
Total	100.00	100.00				

(c)

Figure 7: EDX analysis of different locations on fracture surface A



(a)



(b)

Figure 8: Hardness test locations on the longitudinal cross-section of (a) fracture surface A and (b) fracture surface B.